91-

OPTIMAL CONTROL APPLICATIONS & METHODS, VOL. 13, 121–144 (1992)

TRADE-OFFS IN LINEAR CONTROL SYSTEM DESIGN: A PRACTICAL EXAMPLE

BART DE MOOR, JOHAN DAVID AND JOOS VANDEWALLE
Department of Electrical Engineering, Katholieke Universiteit Leuven, Kardinaal Mercierlaan 94, B-3001 Leuven, Belgium

AND

MAARTEN DE MOOR AND DANIEL BERCKMANS
Department of Agricultural Engineering, Katholieke Universiteit Leuven, Kardinaal Mercierlaan 92, B-3001 Leuven, Belgium

SUMMARY

In this paper two modern control techniques, the H_2 and H_∞ control design methods, are presented. After a brief theoretical explanation they are applied to a practical example: the control of the air flow rate through an axial ventilator. Modern control techniques are model-based. In the first part of the paper it is explained how a model can be obtained both of the process and of the disturbances acting on it. On the basis of the model, several controllers can be designed. The example clearly illustrates some of the trade-offs of modern control design. The H_2 and H_∞ controllers are also compared with a classical PI controller.

KEY WORDS Model-based controllers H_∞ LQG Computer-aided control system design (CACSD)

1. INTRODUCTION

During the last 30 years or so, significant progress has been made in the development of mathematical control design techniques for multivariable systems together with enormous advances in computing power. The available design tools, especially for *linear time-invariant controllers* that stabilize a given linear time-invariant plant and at the same time meet some given engineering specifications, could be of major importance in many industrial applications. Yet, most of these model-driven design techniques are rarely used in everyday practice. This can partly be explained by the need for models and the fact that most relevant systems are *multiple-input/multiple-output* (MIMO). Even when a model has been obtained, using e.g. system identification techniques, the required expertise is significant and should be contrasted with the relatively simple classical tuning rules based on Nyquist and Bode plots and single-loop PID controllers for *single-input/single-output* (SISO) systems.

In this paper we want to compare several designs and show that even when a design is optimal in some sense it can be bad with respect to another criterion: not all criteria can be optimized at the same time. The designer has to find the best controller for his application. Therefore we shall consider the design of a controller as a complete diagnosis of a particular linear system from the linear controller point of view. The designs can then be compared with

0143–2087/92/020121–24$17.00
© 1992 by John Wiley & Sons, Ltd.
Received 25 April 1991
Revised 16 March 1992

respect to several measures such as robustness of certain properties (stability, sensitivity, etc.) or performance issues (disturbance rejection, tracking capabilities, etc.). We will apply this model-based control design and diagnosis to a simple system: the control of the air flow rate through an axial ventilator. The ventilator used is a Siemens 450.

The paper is organized as follows. In Section 2 we describe how a model of the ventilator and the disturbances is obtained. The considered design methods are introduced in Section 3 and then applied to the model of Section 2. In Section 4 some fundamental properties of *linear* systems are illustrated with the example at hand. In Section 5 the different designs are compared. In this section the trade-offs between the different criteria will be highlighted. Finally, in Section 6 some conclusions are summarized. Our notation is fairly standard.

One of our main sources of inspiration is certainly the methodologies explained in References 1–3. We will apply these insights here, however, to a real practical system, namely an industrial ventilator.

We will also demonstrate how software packages for CACSD, such as MATLAB[4] and $MATRIX_X$,[5] are extremely useful in the design and analysis of model-based control strategies.

2. MODELS

The system to be analysed is a ventilator whose control input is the voltage $v(t)$ and regulated output is the air flow rate $f(t)$. Another input is the atmospheric pressure $p(t)$, which acts as a disturbance. The input–output characteristics are non-linear. The overall control objective is set-point control: the flow rate f has to remain as constant as possible despite random pressure variations due to the wind and step-like inputs due to sudden changes in pressure (e.g. when a door is opened). However, because of space limitations, only the pressure disturbance due to the wind is considered. The flow through the ventilator is measured with a flow sensor.

2.1. *Steady state and dynamic model*

Curves of equilibrium triplets (v_{eq}, f_{eq}, p_{eq}) were obtained from static experiments (Figure 1). As a first step in the modelling process, the equilibrium curves were fitted using a non-linear least squares approach. The proposed equilibrium model is

$$f_{eq}(v_{eq}, p_{eq}) = f_\infty \left[1 - \left(\frac{v_0}{v_{eq}}\right)^{1/\eta}\right] \tag{1}$$

where the dead zone v_0, the exponent η and the asymptotic value f_∞ are functions of the pressure p_{eq}. By fitting (1) to each of the experimentally obtained curves of Figure 1, v_0, f_∞ and η were obtained as a function of p_{eq}. Their behaviour as a function of p_{eq} is quite linear* and, using standard linear least squares, the following fits were obtained:

$$f_\infty = 6119 \cdot 6429 - 454 \cdot 4643 p_{eq} \tag{2}$$

$$\eta = 0 \cdot 2548 - 0 \cdot 0129 p_{eq} \tag{3}$$

$$v_0 = 121 \cdot 1429 + 5 \cdot 2143 p_{eq} \tag{4}$$

Our next task is to obtain a dynamic model, the steady state of which coincides with the measured steady state curves. Assume that the ventilator is operating in the neighbourhood of

* Owing to space limitations, we have omitted many figures, which can be found in the corresponding, more complete internal report.[6]

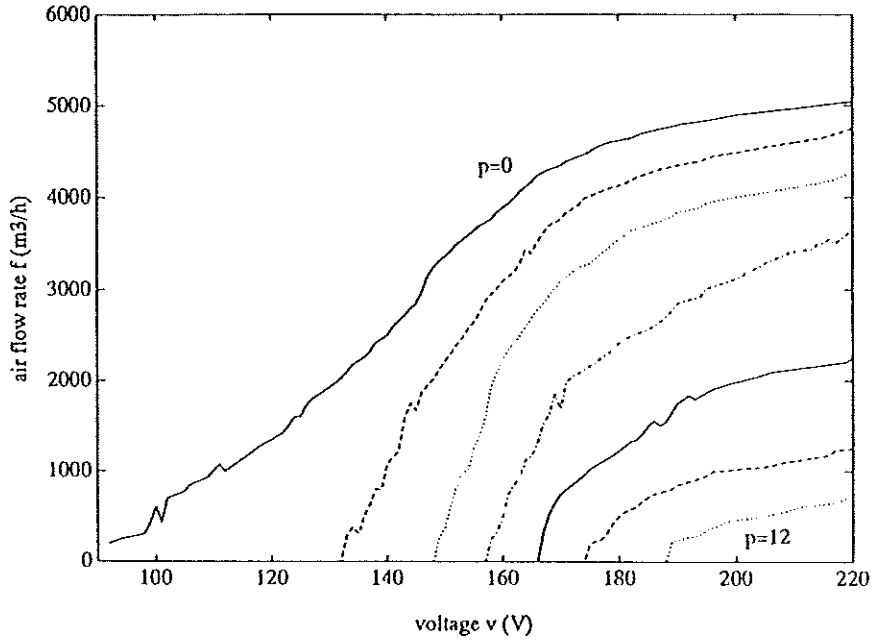


Figure 1. Equilibrium curves of the ventilator for different values of the pressure difference (mm water globe) over the ventilator ($p = 0, 2, 4, 6, 8, 10, 12$)

an equilibrium point ($p_{\text{lin}}, v_{\text{lin}}, f_{\text{lin}}$). We *postulate* that the dynamic behaviour of the system in this neighbourhood can be approximated as

$$\dot{f} = \alpha(f - f_{\text{lin}}) + \beta(v - v_{\text{lin}}) + \gamma(p - p_{\text{lin}}) \tag{5}$$

Define the function c as

$$c(v_{\text{lin}}, p_{\text{lin}}) = \alpha f_{\text{lin}} + \beta v_{\text{lin}} + \gamma p_{\text{lin}} \tag{6}$$

Assume that v and p are constant, say $v = v_{\text{eq}}$ and $p = p_{\text{eq}}$ in the neighbourhood of v_{lin} and p_{lin}, then the flow rate will go towards a new equilibrium given by

$$f_{\text{eq}} = \frac{c}{\alpha} - \frac{\beta}{\alpha} v_{\text{eq}} - \frac{\gamma}{\alpha} p_{\text{eq}} = f_{\text{eq}}(v_{\text{eq}}, p_{\text{eq}}) \tag{7}$$

The second equality is simply the equilibrium function (1). Since v_{eq} and p_{eq} were arbitrary, it follows that

$$\frac{\beta}{\alpha} = -\left.\frac{\delta f_{\text{eq}}}{\delta v_{\text{eq}}}\right|_{v_{\text{lin}}, p_{\text{lin}}} \tag{8}$$

$$\frac{\gamma}{\alpha} = -\left.\frac{\delta f_{\text{eq}}}{\delta p_{\text{eq}}}\right|_{v_{\text{lin}}, p_{\text{lin}}} \tag{9}$$

From some simple step response experiments, for different values of v_{lin} and p_{lin}, it was observed that α is practically independent of v_{lin} and p_{lin}. Thus the coefficients β and γ can be plotted as a function of v_{lin} and p_{lin} using (1), (8) and (9) (Figure 2).

The conclusion is that the ventilator can be modelled as a linear system, the parameters of

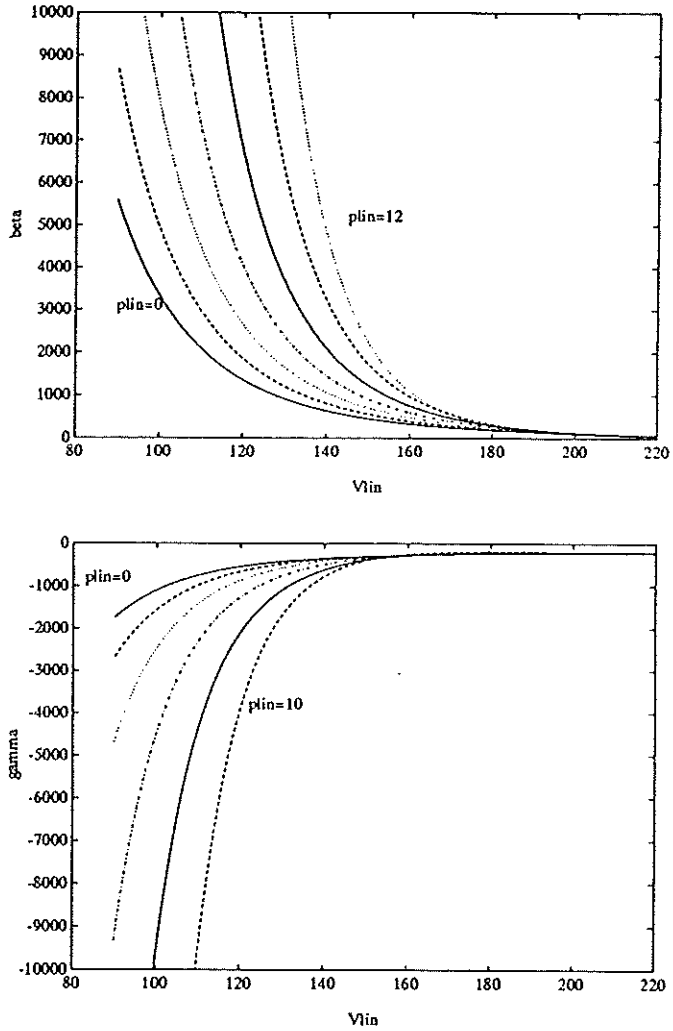


Figure 2. The upper plot shows β and the lower plot γ as a function of v_{lin} (x-axis) and p_{lin} (0, 2, 4, 6, 8, 10, 12)

which vary as a function of the voltage v_{lin} and the pressure p_{lin}. Another point of view could be that we have a linear time-invariant system with bounded uncertainties on the parameters.

Equation (5) can be transformed to a state space model

$$\dot{x}_{\text{p}} = \alpha x_{\text{p}} + \beta v_{\text{l}} + \gamma p_{\text{l}} \tag{10}$$

$$f = x_{\text{p}} + f_{\text{lin}} \tag{11}$$

where $v_{\text{l}} = v - v_{\text{lin}}$ and $p_{\text{l}} = p - p_{\text{lin}}$. The signal p_{l}, which represents variations in pressure due to wind, will be further modelled. Define also $f_{\text{l}} = f - f_{\text{lin}}$, the variations in the air flow rate around the equilibrium. We shall analyse several controllers for the linear model around the equilibrium

$$(v_{\text{lin}}, f_{\text{lin}}, p_{\text{lin}}) = (170,\ 3509,\ 2) \tag{12}$$

The time constant of the ventilator gives us $\alpha = -1/1{\cdot}987 = 0{\cdot}503\,271\,26$ and from equations (8) and (9) $\beta = 21{\cdot}9989$ and $\gamma = -248{\cdot}2494$. Actually, the value of β that will be used is 13 times higher, a factor which comes from a simplified model of a DC/AC conversion.

2.2. *Disturbance model*

A typical disturbance for a ventilator is the wind. A typical spectrum is depicted in Figure 3. The energy appears to be distributed into two regions separated by a distinctive gap. The low-frequency content is centered at approximately 4 days. This corresponds to movement of large-scale pressure systems. There is also a small peak located at diurnal frequency. The high-frequency components may be associated with turbulence and have a peak at approximately 1 cycle min^{-1} ($\frac{1}{60}$ Hz). The magnitude of the high-frequency response depends on the speed of the mean flow. As a matter of fact, the energy in the turbulence appears to be approximately proportional to the square of the average wind speed. Thus in storm wind the spectrum shifts to higher frequencies. The existence of the gap enables a convenient and important distinction to be made between mean wind and fluctuations. The choice of an averaging period for the mean wind of approximately 1 h–10 min duration should provide fairly stable mean values. Since our controller is expected to reject primarily the fast wind disturbances and because of the gap in the wind spectrum, we decide to model only the high-frequency part of the wind spectrum.

In order to obtain a minimum phase SISO transfer function from power spectrum data, observe that the magnitude of a SISO transfer function $G(s)$ evaluated on the imaginary axis $j\omega$, $-\infty \leqslant \omega \leqslant \infty$, is given by

$$|G(s)|^2 = G(s)G(\bar{s}) = G(s)G(-s) \tag{13}$$

for $s = j\omega$. The coefficients of the numerator and denominator polynomials of $G(s)G(\bar{s})$ can be derived from a set of linear equations as explained e.g. in Reference 7. The pole–zero pattern of $G(s)G(\bar{s})$ will exhibit a quadrantal symmetry in the complex plane. This is exploited by taking only the poles and zeros in the left half-plane to construct $G(s)$. A good model for the wind disturbances is obtained with a third-order system driven by white noise. The result of the fit is shown in Figure 4. The obtained model was then scaled to make its 2-norm equal

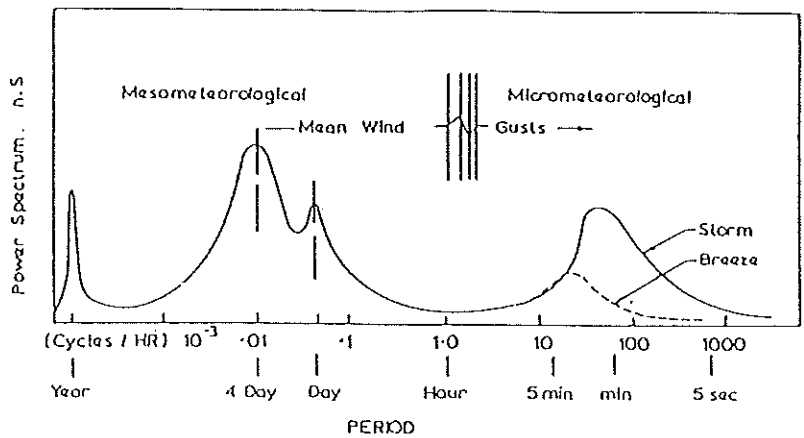


Figure 3. The spectrum of the wind

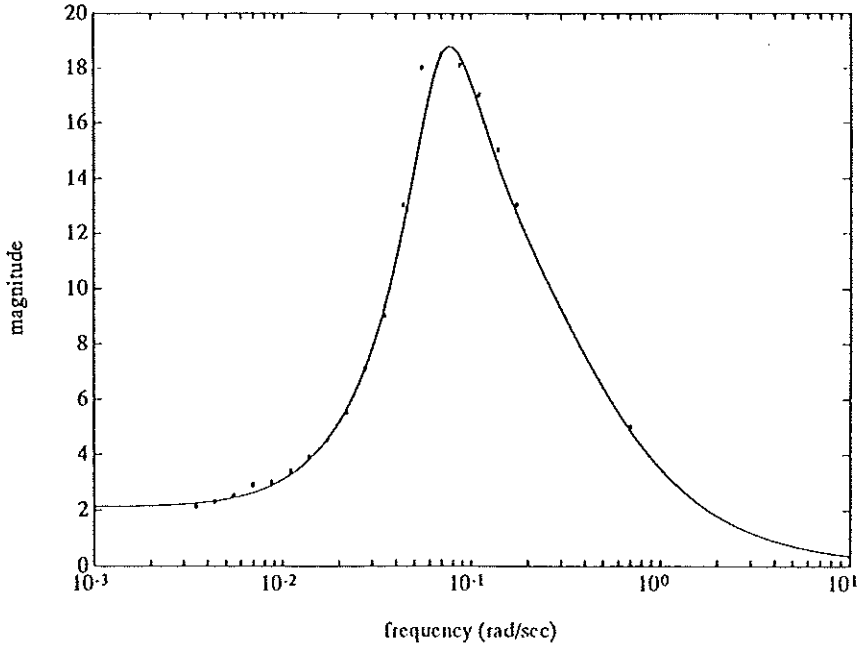


Figure 4. The fit of the wind spectrum: (dots, measured; full curve, model)

to one. The resulting model is

$$\dot{x}_d = \mathbf{A}_d x_d + \mathbf{B}_d w_d \tag{14}$$

$$p_1 = \mathbf{C}_d x_d + \mathbf{D}_d w_d \tag{15}$$

with

$$\mathbf{A}_d = \begin{bmatrix} -3{\cdot}6425 \times 10^{-1} & -2{\cdot}6070 \times 10^{-2} & -1{\cdot}4078 \times 10^{-3} \\ 1{\cdot}0000 \times 10^{0} & 0{\cdot}0 & 0{\cdot}0 \\ 0{\cdot}0 & 1{\cdot}0000 \times 10^{0} & 0{\cdot}0 \end{bmatrix} \tag{16}$$

$$\mathbf{B}_d = \begin{bmatrix} 4{\cdot}3748 \times 10^{-1} \\ 0{\cdot}0 \\ 0{\cdot}0 \end{bmatrix} \tag{17}$$

$$\mathbf{C}_d = [1{\cdot}5826 \times 10^{0} \quad 1{\cdot}5137 \times 10^{-1} \quad 1{\cdot}3044 \times 10^{-3}] \tag{18}$$

$$\mathbf{D}_d = 0 \tag{19}$$

The signal w_d is assumed to be zero-mean Gaussian white noise with variance $\sigma^2_{w_d} = 1$.

2.3 Measurements

The measurement of the flow rate f is modelled as a first-order linear dynamical system with additive measurement noise:

$$\dot{x}_m = \alpha_m x_m + \beta_m f \tag{20}$$

$$v_m = \gamma_m x_m + \delta_m w_m \tag{21}$$

Since measuring a flow rate is quite difficult, we model the inaccuracy of the measurements by additive zero-mean Gaussian white noise with variance $\sigma^2_{w_m} = 100$. The variance is derived from the known accuracy of the sensor around the equilibrium point (12).

The output v_m is a voltage which will be fed back to the input via a controller. From experiments on the measurement equipment the following values were obtained.

$$\alpha_m = -1/5 \cdot 5820, \qquad \beta_m = 0 \cdot 06270 \tag{22}$$

$$\gamma_m = 1/140, \qquad \delta_m = 1/140 \tag{23}$$

2.4 Controller

The controller has to keep the air flow rate through the ventilator, f_{lin}, constant. This will be called the set-point. Using equations (20) and (21), the desired air flow rate is converted into an *equivalent* voltage v_{ref}. In the noiseless case, $w_m = 0$, we would like that in equilibrium the set-point $v_{ref} = v_m$. Hence

$$v_{ref} = -\frac{\gamma_m \beta_m}{\alpha_m} f_{lin} \tag{24}$$

The error signal $e(t)$ is obtained as

$$e = v_{ref} - v_m \tag{25}$$

In general the controller will be represented by the state space model

$$\dot{x}_c = \mathbf{A}_c x_c + \mathbf{B}_c e \tag{26}$$

$$v_I = \mathbf{C}_c x_c + \mathbf{D}_c e \tag{27}$$

2.5. The generalized plant

The different models we have obtained will now be combined in a generalized plant. To explain the concept of the generalized plant, we first need some definitions. The inputs to any kind of plant can always be divided into two vector signals.

(i) The *actuator signal vector*, denoted by u, consists of the inputs to the model that can be *manipulated* by the controller.
(ii) The *exogenous input vector*, denoted by w, consists of all other input signals to the model.

Similarly, the outputs of the model consist of two vector signals.

(i) The *sensor signal vector*, denoted y, consists of output signals that are accessible to the controller.
(ii) The *regulated outputs signal vector*, denoted z, consists of every signal from the model which is of interest to the designer.

The model of the system with the two vector input signals w and u and the two vector output signals z and y is referred to as the *generalized plant* **P**, shown in Figure 5.

Four linear transfer functions are defined, $\mathbf{P}_{11}$, $\mathbf{P}_{12}$, $\mathbf{P}_{21}$ and $\mathbf{P}_{22}$, such that

$$\begin{bmatrix} \mathbf{z} \\ \mathbf{y} \end{bmatrix} = \begin{bmatrix} \mathbf{P}_{11} & \mathbf{P}_{12} \\ \mathbf{P}_{21} & \mathbf{P}_{22} \end{bmatrix} \begin{bmatrix} \mathbf{w} \\ \mathbf{u} \end{bmatrix}$$

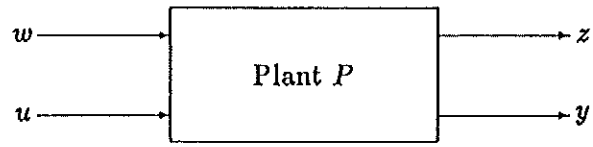


Figure 5. The plant inputs are partitioned into signals that can be manipulated by the controller (u) and signals not manipulated by the controller (w). The outputs are divided into ones accessible by the controller (y) and the controlled outputs of the plant (z)

For example, $\mathbf{P}_{22}$ is the transfer function from controller input **u** to the sensed outputs **y**. If a controller is present, the closed-loop system is as shown in Figure 6. The closed-loop transfer function **G** is then

$$\mathbf{G} = \mathbf{P}_{11} + \mathbf{P}_{12}\mathbf{C}(\mathbf{I} - \mathbf{P}_{22}\mathbf{C})^{-1}\mathbf{P}_{21} \tag{28}$$

Combining the models of the ventilator, the wind and the sensor, the block diagram of Figure 7 is obtained. The dashed box is our generalized plant. The inputs and outputs can be

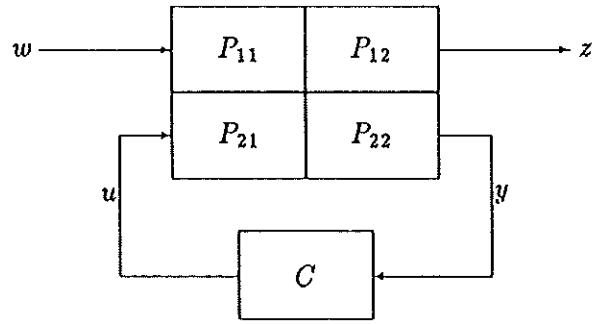


Figure 6. The closed-loop system. The controller processes the sensed signals y to produce the actuator signals u

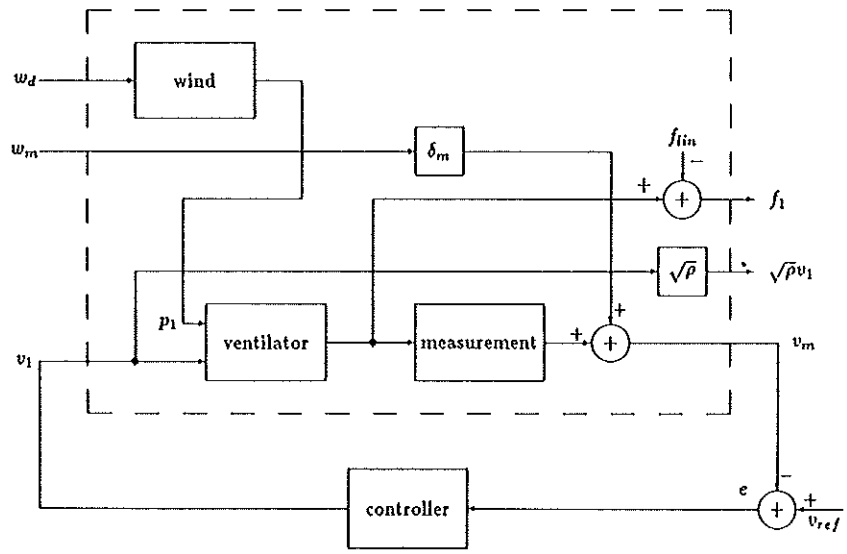


Figure 7. The block diagram of the ventilator configuration

defined as

$$\textit{external inputs} \quad \mathbf{w} = [w_d \;\; w_m]^T$$
$$\textit{controller input} \quad \mathbf{u} = v_1$$
$$\textit{output to be minimized} \quad \mathbf{z} = [f_1 \;\; \sqrt{\rho} v_1]^T$$
$$\textit{measurement output to the controller} \quad \mathbf{y} = v_m$$

The output vector $\mathbf{z}$ contains all the signals to be controlled. Therefore the controlled output $\mathbf{z}$ does not not only contain the air flow rate variations f_1, but also the actuator output v_1. The controller energy should not be too excessive. The controller output is also scaled with a parameter $\sqrt{\rho}$ to influence the allowed control energy. This is used in later experiments.

The resulting generalized model for this example is therefore given by*

$$\begin{bmatrix} \mathbf{P}_{11} & \mathbf{P}_{12} \\ \mathbf{P}_{21} & \mathbf{P}_{22} \end{bmatrix} = \left[\begin{array}{c|cc} \mathbf{A} & \mathbf{B}_1 & \mathbf{B}_2 \\ \hline \mathbf{C}_1 & \mathbf{D}_{11} & \mathbf{D}_{12} \\ \mathbf{C}_2 & \mathbf{D}_{12} & \mathbf{D}_{22} \end{array}\right]$$

$$= \left[\begin{array}{ccccc|cc|c} -0{\cdot}5033 & -392{\cdot}8866 & -37{\cdot}5781 & -0{\cdot}3238 & 0 & 0 & 0 & 286{\cdot}0103 \\ 0 & -0{\cdot}3643 & -0{\cdot}0261 & -0{\cdot}0014 & 0 & 0{\cdot}4375 & 0 & 0 \\ 0 & 1{\cdot}0000 & 0 & 0 & 0 & 0 & 0 & 0 \\ 0 & 0 & 1{\cdot}0000 & 0 & 0 & 0 & 0 & 0 \\ 0{\cdot}0627 & 0 & 0 & 0 & -0{\cdot}1791 & 0 & 0 & 0 \\ \hline 1{\cdot}0000 & 0 & 0 & 0 & 0 & 0 & 0 & 0 \\ 0 & 0 & 0 & 0 & 0 & 0 & 0 & \sqrt{\rho} \\ \hline 0 & 0 & 0 & 0 & -0{\cdot}0071 & 0 & -0{\cdot}0071 & 0 \end{array}\right] \tag{29}$$

where the five states are due to one plant state, three states of the wind model and one state of the measurement.

3. CONTROLLERS

In this section the design of the controllers is discussed. Three controllers were compared: a PI controller, an H_2 controller and an H_∞ controller. The first constraint they all have to satisfy is to *stabilize* the closed-loop system.

3.1. PI control

We shall restrict ourselves to PI controllers and omit the derivative action (as is often done in industry). A PI controller is a first-order dynamic system with state space representation

$$\dot{z}_c = 0 z_c + k_1 e \tag{30}$$

$$u = z_c + k_2 e \tag{31}$$

Here k_1 is the integral constant and k_2 is the proportional constant. Assume that there is no wind ($p_1 = 0$). The characteristic equation of the closed-loop system consisting of the plant, the sensor and the PI controller is easily found to be

$$s^3 - (\alpha + \alpha_m)s^2 + (\alpha\alpha_m + \beta\gamma_m\beta_m k_2)s + \beta\gamma_m\beta_m k_1 = 0 \tag{32}$$

* $\mathbf{P}_{ij}$ is defined as $\mathbf{P}_{ij} = \mathbf{C}_i(s\mathbf{I} - \mathbf{A})\mathbf{B}_j + \mathbf{D}_{ij}$.

The stability of the closed-loop system can be investigated using a classical Routh table test,[8] which results in

$$k_1 < \frac{k_2}{1{\cdot}4653} + \frac{137{\cdot}38}{\beta} \tag{33}$$

The transfer function of the PI controller can be written as

$$C(s) = K_c\left(1 + \frac{1}{\tau_i s}\right) \tag{34}$$

where

$$K_c = k_2, \qquad \tau_i = k_2/k_1$$

To tune a PID controller, the best-known rules are those of Ziegler and Nichols, which are, however, only applicable on SISO plants. The system we want to regulate here is the one from v_1, the voltage input of the ventilator, to e, the measured deviation from the set-point. Applying the Ziegler–Nichols rules to this system yields[9]

$$K_c = 7{\cdot}82, \qquad \tau_i = 2{\cdot}57$$

From K_c and τ_i the values of k_1 and k_2 of the state space realization (31) can be determined as

$$k_1 = 3{\cdot}04, \qquad k_2 = 7{\cdot}82$$

These satisfy the inequality (33) of the Routh–Hurwitz criterion.

In Figure 8 we show a singular value plot* as a function of frequency of the closed-loop

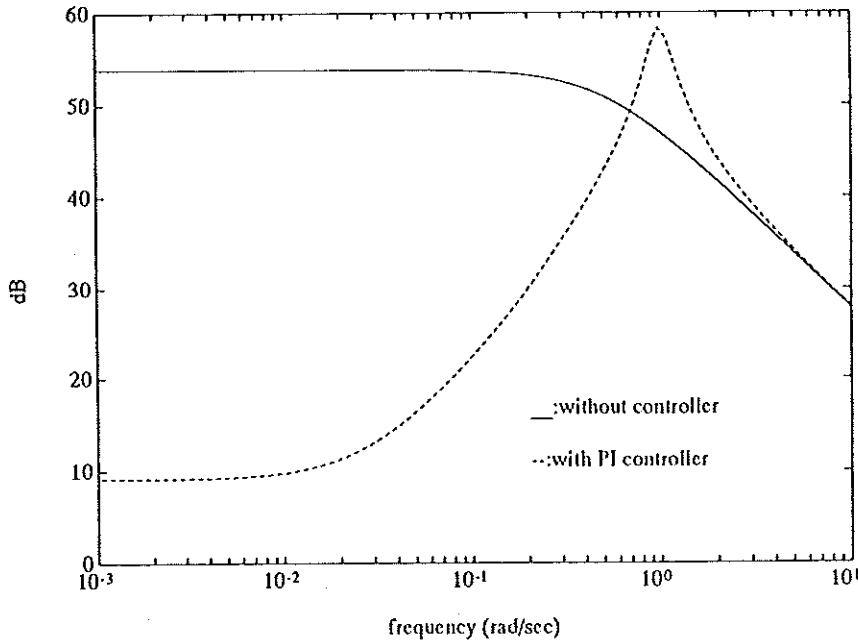


Figure 8. The dashed lines is the singular value plot of the closed loop with PI controller from $[p_1 \ w_m]^T$ to f_1. The full line is the magnitude plot of the ventilator from p_1 to f_1

* The singular value plot is a multivariable generalization of the magnitude plot of a transfer function for SISO systems. It shows the singular values of the transfer matrix as a function of frequency.

transfer function from the disturbances $[p_1 \ w_m]^T$ to f_1. Obviously, for good disturbance rejection the singular values should be small.

3.2. H_2 optimal control design

The 2-norm of a MIMO system is defined as

$$\| \mathbf{G} \|_2^2 = \frac{1}{2\pi} \int_{-\infty}^{\infty} \text{trace}(\mathbf{G}^*(j\omega)\mathbf{G}(j\omega)) \, d\omega \tag{35}$$

The 2-norm of the transfer function is a measure of the power in the output of the system when the input is white noise with unit power. Similarly, it is the RMS of the output signal for a white noise input signal, with covariance matrix equal to the identity.

The H_2 optimal control design problem for our purpose can be formulated as

$$\min_{\text{over all stabilizing controllers } \mathbf{C}(s)} \| \mathbf{G} \|_2 \tag{36}$$

where $\mathbf{G} = \mathbf{P}_{11} + \mathbf{P}_{12}\mathbf{C}(\mathbf{I} - \mathbf{P}_{22}\mathbf{C})^{-1}\mathbf{P}_{21}$.

The solution of the H_2 control problem is based on two algebraic Riccati equations. More details can be found in References 10–12.

For the generalized plant (29) given in Section 2.5 the optimal H_2 controller can be calculated. However, to take into account the different variances of the white noise inputs w_d and w_m, the inputs are multiplied by σ_{w_d} and σ_{w_m} respectively. The factor ρ that scales the energy output in the H_2 design serves as a design parameter. Increasing ρ decreases the allowed energy in the output of the controller and vice versa. In this way the whole design is influenced by changing ρ, which will be shown extensively below. It is up to the designer to choose a suitable ρ that gives a reasonable trade-off between the different design specifications.

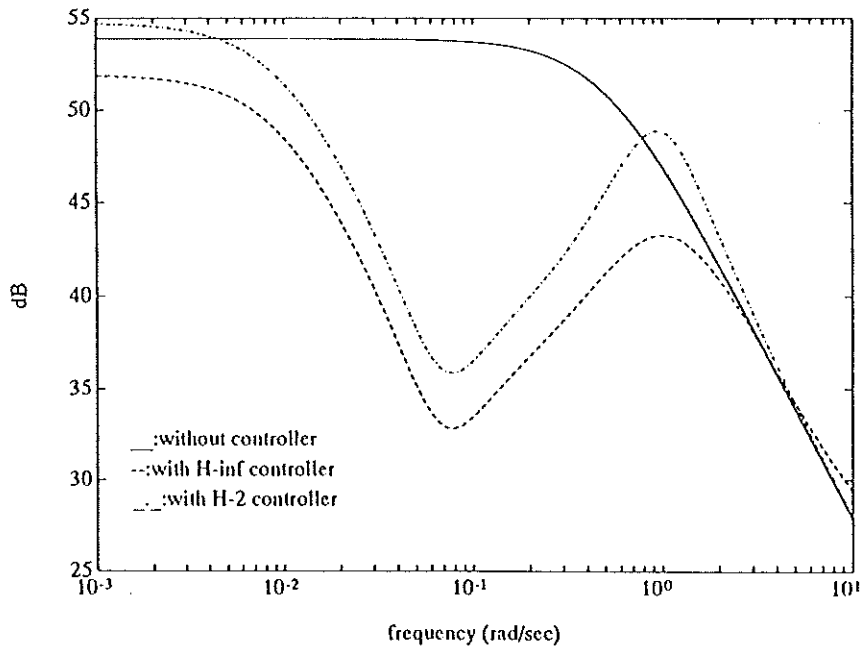


Figure 9. The transfer function of $[p_1 \ w_m]^T$ to f_1 with H_2 and H_∞ controllers ($\rho = 1$)

The singular value plot of the closed-loop transfer function from $[p_1 \ w_m]^T$ to f_1 is shown in Figure 9 (for $\rho = 1$). From the plot it is clear that the H_2 controller compensates for the disturbances at which the wind spectrum is the largest. Hence we have fairly good disturbance rejection. The state space realization of the H_2 controller is

$$\left[\begin{array}{c|c} \mathbf{A}_c & \mathbf{B}_c \\ \hline \mathbf{C}_c & \mathbf{D}_c \end{array}\right] = \left[\begin{array}{ccccc|c} -286 & -1{\cdot}059 & -0{\cdot}1007 & -0{\cdot}002498 & -15{\cdot}25 & -2136 \\ 0 & -0{\cdot}3643 & -0{\cdot}02607 & -0{\cdot}001408 & 0{\cdot}01984 & 2{\cdot}778 \\ 0 & 1 & 0 & 0 & 0{\cdot}06023 & 8{\cdot}432 \\ 0 & 0 & 1 & 0 & 0{\cdot}07063 & 9{\cdot}888 \\ 0{\cdot}0627 & 0 & 0 & 0 & -1{\cdot}395 & -170{\cdot}2 \\ \hline -0{\cdot}9982 & 1{\cdot}37 & 0{\cdot}131 & 0{\cdot}001124 & 0 & 0 \end{array}\right] \tag{37}$$

3.3. H_∞ controllers

The optimal H_∞ controller minimizes the ∞-norm, which is defined as

$$\| \mathbf{F}(s) \|_\infty = \sup_s (\sigma_{\max}(\mathbf{F}(s))) \quad \forall \mathrm{Re}(s) > 0 \tag{38}$$

Here $\sigma_{\max}$ is the maximum singular value of the matrix between parentheses.

The ∞-norm is only defined for stable matrix functions. A stable transfer function has no poles in the closed right half-plane. By the maximum modulus theorem the ∞-norm can then be written as

$$\| \mathbf{F}(s) \|_\infty = \sup_\omega (\sigma_{\max}(\mathbf{F}(j\omega))) \quad \forall \omega \tag{39}$$

The ∞-norm can easily be seen on a Bode plot: it is the magnitude of the maximum value of the largest singular value. Look e.g. at Figures 8 and 9. The ∞-norm is a measure of the worst possible energy amplification of a signal from the input to the output.

Because the H_∞ controller can take into account the peak values of e.g. the disturbances, it can be made robust to the disturbances. If a class of disturbances is known, a specific H_∞ controller can be designed that will stabilize the system for any disturbance of the given class, at the price of a certain conservatism.

The first solutions to the H_∞ design problem involved quite complicated computation methods based on factorizations and Nehari approximations.[11,13] More recently, it was shown how to solve the H_∞ control problem using the solution of two Riccati equations which makes the calculations quite similar to those of the H_2 controller. They are described e.g. in References 14–16. The solution to the H_∞ control problem is not unique, but there is a whole set of solutions. All stabilizing H_∞ controllers can be parametrized in a linear fractional map with the feedback as a parameter.

For our purpose we propose to solve the following H_∞ control problem:

$$\min_{\text{over all stabilizing controllers } \mathbf{C}(s)} \| \mathbf{P}_{11} + \mathbf{P}_{12}\mathbf{C}(\mathbf{I} - \mathbf{P}_{22}\mathbf{C})^{-1}\mathbf{P}_{21} \|_\infty$$

A controller that solves the H_∞ control problem is found by iteration. For different values of

γ,* one checks if there exists a controller such that

$$\| \mathbf{P}_{11} + \mathbf{P}_{12}\mathbf{C}(\mathbf{I} - \mathbf{P}_{22}\mathbf{C})^{-1}\mathbf{P}_{21} \|_\infty < \gamma$$

The lowest γ for which there exists a controller is called the optimal γ, γ_{opt}. If no controller can be found for γ, then $\gamma < \gamma_{opt}$. If a controller exists, then $\gamma > \gamma_{opt}$. Using a bisection algorithm, it is possible to approximate γ_{opt} as closely as desired.

The optimal H_∞ controller is based on the generalized plant (29) of Section 2.5. Again the inputs w_d and w_m are multiplied by σ_{w_d} and σ_{w_m} respectively to take into account the variances.

The H_∞ controller shown below is the so-called central controller of the set of H_∞ controllers. γ_{opt} was calculated within a relative accuracy of 10^{-7}. The resulting γ is $\gamma = 159{\cdot}66$. The state space model of the controller is

$$\left[\begin{array}{c|c} \mathbf{A}_c & \mathbf{B}_c \\ \hline \mathbf{C}_c & \mathbf{D}_c \end{array}\right] = \left[\begin{array}{cccc|c} -0{\cdot}1811 & -3{\cdot}11 & -0{\cdot}7282 & -0{\cdot}7139 & 457{\cdot}3 \\ 4{\cdot}421 & -254{\cdot}7 & -59{\cdot}92 & -58{\cdot}65 & 3{\cdot}745 \times 10^4 \\ 1{\cdot}684 & -61{\cdot}3 & -15 & -14{\cdot}79 & 9053 \\ 2{\cdot}273 & -77{\cdot}82 & -17{\cdot}94 & -17{\cdot}49 & 1{\cdot}142 \times 10^4 \\ \hline 1{\cdot}662 & -15{\cdot}16 & -3{\cdot}595 & -3{\cdot}525 & 2235 \end{array}\right] \quad (40)$$

The result is shown in Figure 9 ($\rho = 1$). The singular value plot of the closed-loop transfer function with an H_∞ controller is slightly lower than the one with an H_2 controller.

A disadvantage of the H_2 and H_∞ controllers is that they are both of a higher order than the PI controller. Both have the same order as the generalized plant, i.e. five. This makes the implementation harder. Model reduction could be considered. However, owing to space limitations, this is not further explained. The interested reader is referred to e.g. References 10 and 17–19.

4. FUNDAMENTAL PROPERTIES OF LINEAR SYSTEMS

In this section we will illustrate some fundamental properties of *linear time-invariant* controllers for *linear time-invariant* systems using our ventilator example.

4.1. Bode integral

One of the constraints on the design of a *linear* controller is the Bode integral. Already in 1945 Bode proved for a stable rational SISO plant P and controller C that†

$$\int \log | H_{yd} | \, d\omega = 0 \quad (41)$$

where H_{yd} is the disturbance rejection transfer function, $H_{yd} = (I + PC)^{-1}$. This formula only holds for stable P and C, with $PC = O(s^{-2})$. An interpretation is that regions with disturbance rejection ($\log | H_{yd} | < 0$) are compensated by regions with disturbance amplification ($\log | H_{yd} | > 0$). Asking for more disturbance rejection in one frequency range will also result in disturbance amplification in other ranges. In the case of the standard plant, take

* This γ is different from the γ used in the model of the ventilator. However, because γ is used in most literature on H_∞ control, it is also used here.

† This result of Bode was generalized by Boyd and Desoer for MIMO systems to[20] $\int \log \| \mathbf{H}_{yd}(j\omega) \| \, d\omega \geq 0$, where $\| \cdot \|$ denotes any induced norm, e.g. the largest singular value of the matrix.

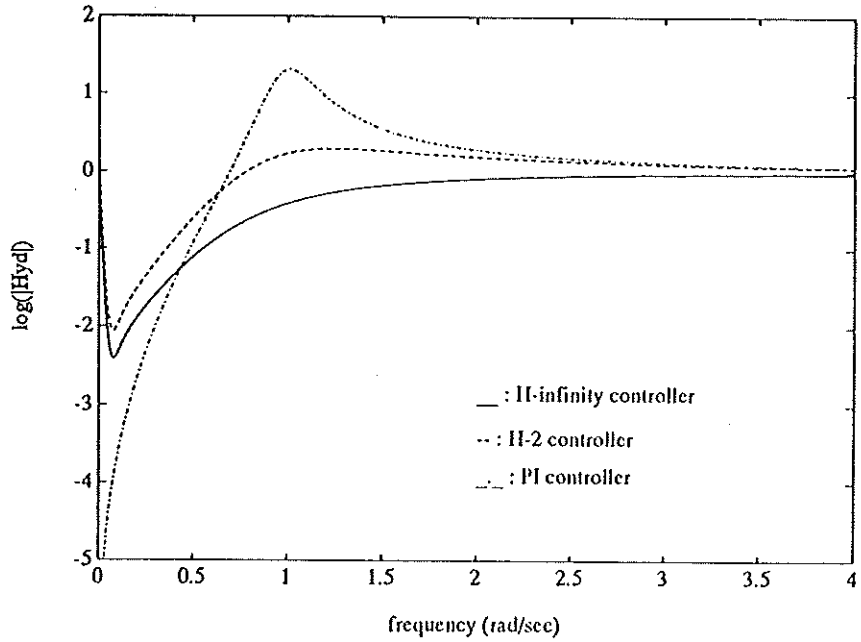


Figure 10. The logarithm of the magnitude of the sensitivity function $(I - P_{22}C)^{-1}$ as a function of frequency

$H_{yd} = (I - P_{22}C)^{-1}$, where P_{22} is the transfer function from u to y. Then equation (41) also holds.

This is illustrated in Figure 10 for the ventilator. For the H_∞ controller it is not clear that (41) holds. However, there is a large interval at higher frequencies where $\log |H_{yd}|$ is slightly above zero. This compensates the negative area at low frequencies.

4.2. *The internal model theorem*

The *internal model theorem* states that a controller always carries an approximation of the inverse of the plant which has to be controlled.[21] This is easily explained. Consider the classical closed-loop transfer function

$$T = PC(I + PC)^{-1} \tag{42}$$

Introduce now the Q-parametrization

$$Q = C(I + PC)^{-1} \tag{43}$$

Substituting (43) in (42) results in

$$T = PQ \tag{44}$$

From (43) it follows that

$$C = (I - QP)^{-1}Q \tag{45}$$

If we want T close to unity, then $Q \approx P^{-1}$. This also explains that some trouble is to be expected if the plant has non-minimum phase zeros, which is, however, not the case for our example.

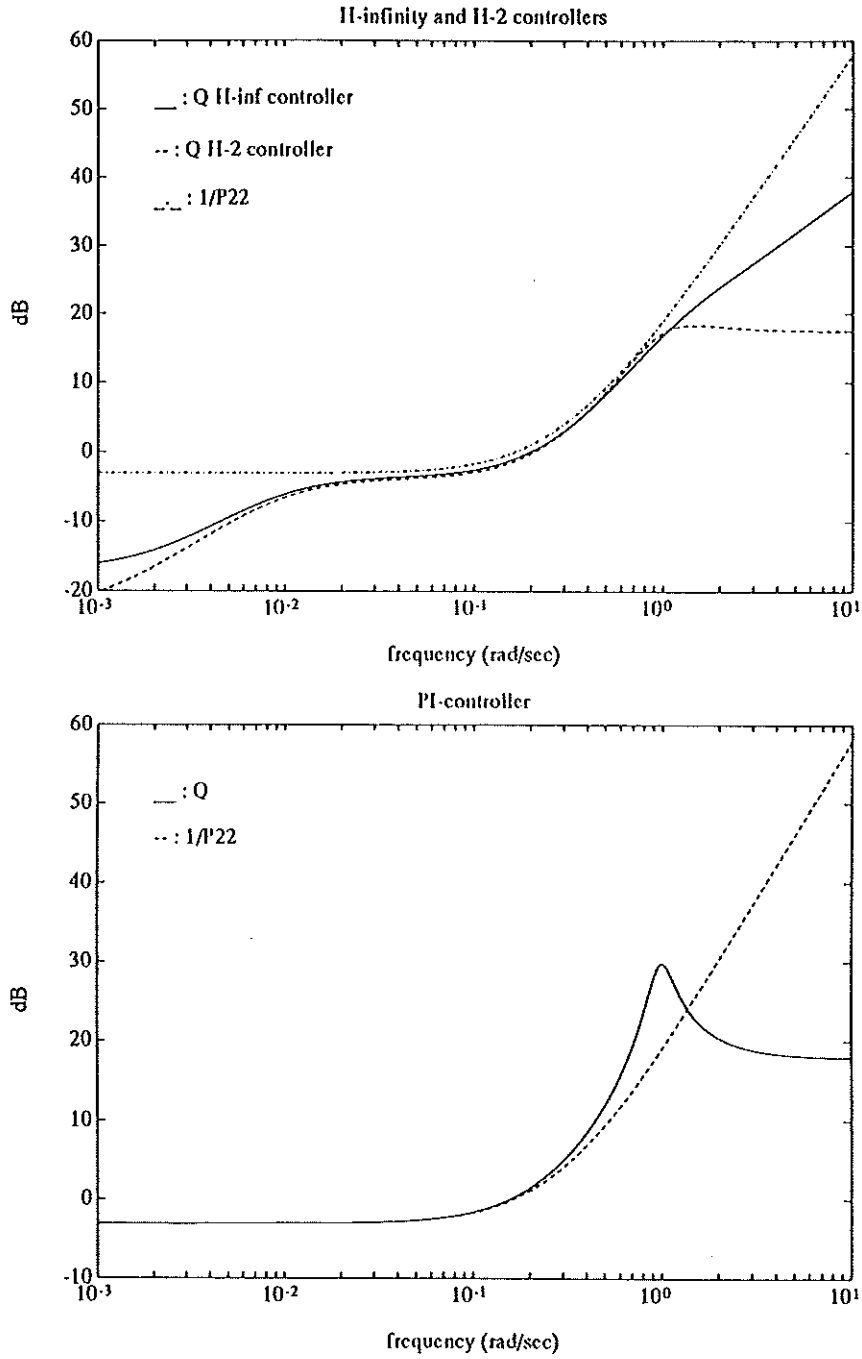


Figure 11. The logarithm of the magnitude of P_{22}^{-1} and $Q = C(I - P_{22}C)^{-1}$ for the different controllers

In Figure 11 the logarithmic magnitudes of P_{22}^{-1}, where P_{22} is the transfer function from v_1 to e, and $Q = C(I + P_{22}C)^{-1}$ (positive feedback is used) are plotted. For the PI controller of Section 3.1 it is clear that for low frequencies Q coincides with P_{22}^{-1}. In Figure 11 the Qs of the H_∞ and H_2 controllers are also shown. The approximations are worse than in the case of the PI controller. The inverse is approximated best where the wind disturbance is largest. The wind disturbance model acts here as a weighting function of the input w_d. The conclusion is thus that Q still approximates the inverse but only in the frequency range where the weight is strong enough.

5. PERFORMANCE EVALUATION

In this section we discuss some performance criteria, including robustness, sensitivity and disturbance rejection and RMS. Not all of these criteria can be optimized simultaneously. There are trade-offs between different criteria.

5.1. Robustness

A property is called robust if it is conserved in the face of uncertainty, i.e. for a whole range of systems in some neighbourhood of the nominal system. One of the typical problems is to preserve stability of the closed-loop system when disturbances and component variations are imposed. Controller design is often model-based. However, this model is never perfect. There are always modelling errors or ignored plant dynamics, e.g. when a high-dimensional system is approximated with a lower-order model. However, when the controller is applied to the real plant, the closed loop has to be stable. Thus the controller has to be robust also in the face of these uncertainties.

Classically, the robustness of SISO systems is characterized by gain and phase margins. In modern control theory there are several ways to represent plant uncertainty. The plant uncertainty can be structured or unstructured (see e.g. Reference 22). We will only discuss two measures for unstructured uncertainties: the M-circle and the D-circle.

The M-circle is a measure of robustness which combines the gain and phase margins. For SISO systems it can be defined as the minimum distance from the Nyquist plot of the loop gain $\mathbf{L} = \mathbf{PC}(j\omega)$ (or $\mathbf{P}_{22}\mathbf{C}$) to the critical point -1. If M is small, then slight variations could change the number of encirclements of -1 by the loop gain, resulting in an unstable closed-loop system.

The M-circle is related to the maximum sensitivity of the control system by

$$M = \frac{1}{\| \mathbf{S} \|_\infty} \tag{46}$$

where $\mathbf{S} = (\mathbf{1} + \mathbf{PC})^{-1}$ is the *sensitivity transfer function*. Thus a small M-circle corresponds to a peak of the sensitivity function at some frequency. Observe that $(\sigma_{\max}(\mathbf{I} + \mathbf{PC})^{-1})^{-1} = \sigma_{\min}(\mathbf{I} + \mathbf{PC})$. Hence, in order to get M large, we should design the controller in such a way that $\sigma_{\min}(\mathbf{I} + \mathbf{PC})$ is large or, according to popular control design beliefs, that the *loop gain* $\mathbf{PC}$ is large, i.e. $\sigma_{\min}(\mathbf{PC})$ large!

Another measure of robustness concerns the ability of the regulator to maintain closed-loop stability in the face of additive plant perturbations $\Delta\mathbf{P}$. What is the smallest (in the sense of maximum magnitude of frequency response) stable additive perturbation $\Delta\mathbf{P}$ which destabilizes the system? It can be proved that[1]

$$D = \min_{\Delta\mathbf{P} \text{ destab. system}} \| \Delta\mathbf{P} \|_\infty = (\| \mathbf{C}(\mathbf{I} + \mathbf{PC})^{-1} \|_\infty)^{-1} \tag{47}$$

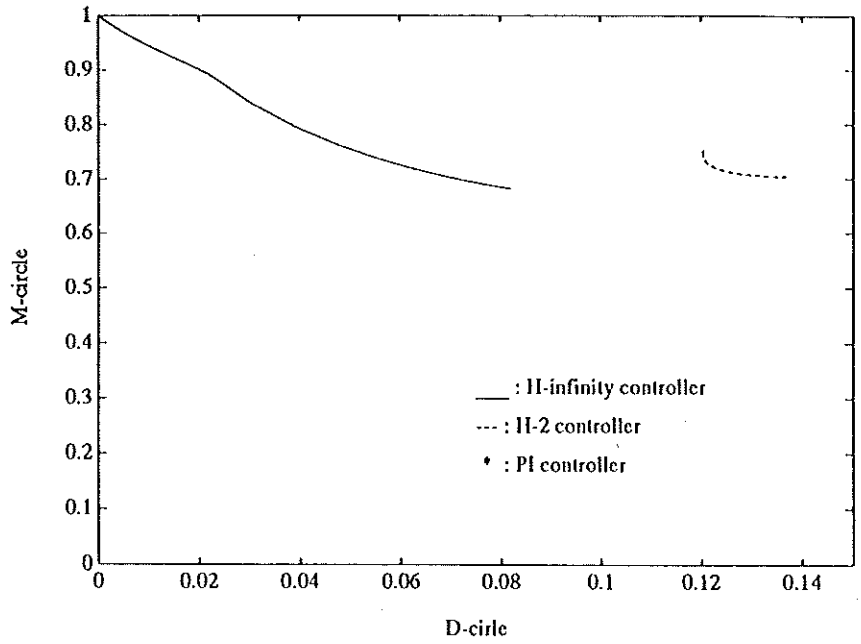


Figure 12. The M-circle and D-circle as a function of ρ. Different H_∞ and H_2 controllers were calculated for ρ varying from 10^{-4} to 10^4. The M-circle and D-circle of the PI controller are given as a reference. Increasing ρ increases the D-circle but decreases the M-circle

which is the inverse of the maximum of the maximum singular value of the transfer function from the reference input to the actuator output.

In general, the robustness requirements that M and D be large are conflicting. A system may have good margins (i.e. large M) but be quite sensitive to additive perturbations (i.e. small D) and vice versa. This is nothing else than another manifestation of trade-offs in control system design. $\mathbf{P}_{22}$ is here the transfer function from v_1, the voltage input of the controller, to e, the output of the flow measure. The M-circle is the smallest distance of the Nyquist plot to the point (1,0).* Thus the larger the M-circle is, the better. Most designs tend to zero when $\omega \to \infty$. Therefore, when the M-circle is close to unity, it is less likely it will become unstable to additive loop perturbations. The D-circle is a measure of the additive plant disturbances. The larger the D-circle, the larger the disturbance can be without destabilizing the closed loop.

The M-circle and D-circle also depend on the parameter ρ. On the plots it will be clear that there is a trade-off between them. A good M-circle will lead to a worse D-circle and vice versa. In Figure 12 the M- and D-circle values are defined as a function of ρ, where ρ varies from 10^{-4} to 10^4.

For low values of ρ the M-circle is large and the D-circle is small. Increasing ρ increases the D-circle but decreases the M-circle. Thus increasing the D-circle makes the closed loop more robust against additive plant perturbations but less robust for open-loop perturbations. It is also obvious that the PI controller is not robust at all. Its M-circle is too small and its D-circle is also small compared to the H_∞ and H_2 controllers.

* The feedback sign convention is positive in this paper. Thus the system becomes unstable if the point (1,0) is encircled on the Nyquist diagram.

5.2. Sensitivity and disturbance rejection

The sensitivity function S is classically defined as

$$S = (I + PC)^{-1} \tag{48}$$

In the case of a generalized plant this can still be used if only the closed loop is considered: take P_{22} instead of P. The sensitivity function shows how well disturbances are rejected. The ∞-norm of the sensitivity function is also the inverse of the M-circle. The lower the norm is, the better the M-circle.

In Figure 13 the magnitudes of the sensitivity functions of the different controllers are plotted for $\rho = 1$. The PI controller has the lowest sensitivity at low frequencies and thus the best disturbance rejection. However, the PI controller also has the largest peak value and as a consequence the lowest M-circle (see Figure 12). A disturbance with that frequency is amplified most. The H_2 and H_∞ controllers have the lowest sensitivity in the region where the wind disturbance model has a large magnitude.

In Figure 14 the sensitivity functions of the H_2 and H_∞ controllers are plotted for different values of ρ. For the H_∞ controllers the sensitivity is not influenced much by ρ if ρ is low. A high ρ, however, makes the sensitivity worse for most frequencies. Then only the frequencies with the largest magnitudes of the spectrum of the wind are filtered out. Similar results can be observed for the H_2 controller. However, for the H_2 controller with a large ρ there is no improvement in the disturbance rejection at the largest magnitudes of the wind spectrum.

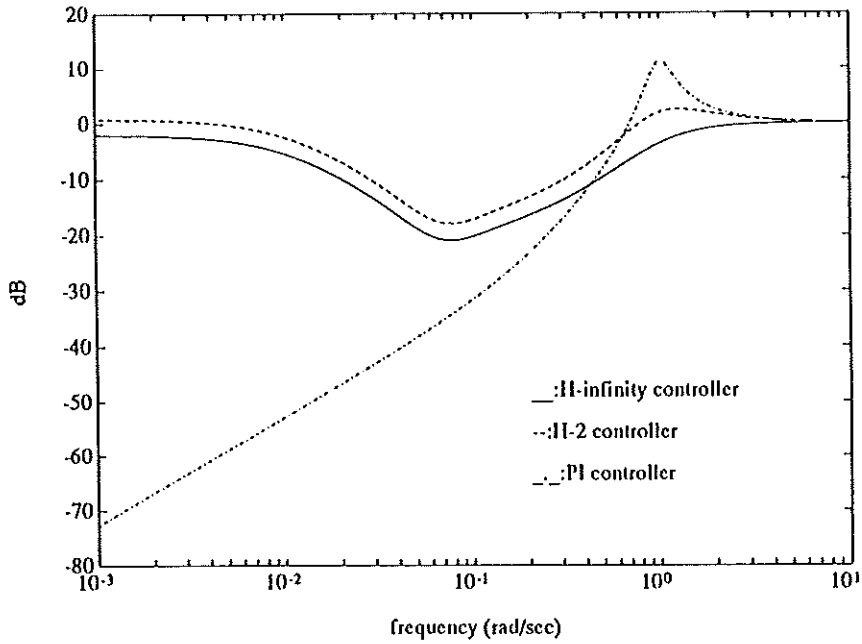


Figure 13. The logarithm of the magnitude of the sensitivity function $(I + P_{22}C)^{-1}$ as a function of frequency for the different controllers ($\rho = 1$)

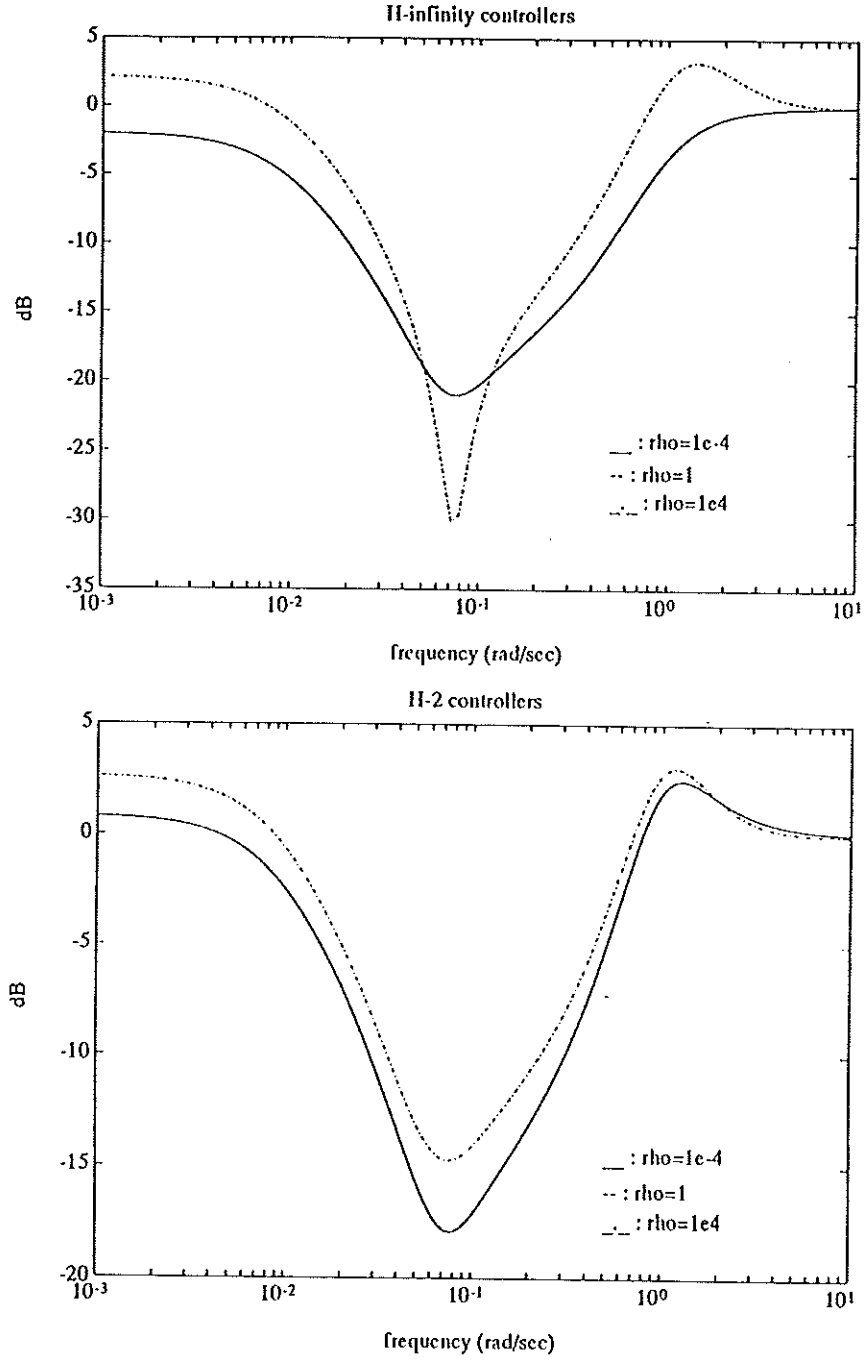


Figure 14. The sensitivity function of H_∞ and H_2 controllers for three values of ρ. There is no difference for $\rho = 10^{-4}$ and $\rho = 1$. Observe the influence of high control energy weighting. A large ρ improves the sensitivity of the closed loop with the H_∞ controller in the interval of large magnitude of the wind spectrum. This is not the case for the H_2 controller

5.3. Trade-off between achievable RMS norms

Using Parseval's theorem, the H_2 cost function (36) can also be written as

$$\int_0^\infty (f_1(t)^2 + \rho v_1(t)^2)\, dt \tag{49}$$

Changing ρ will thus emphasize or de-emphasize the relative importance of the controller energy with respect to the disturbance rejection in the output. The RMS norm of the output signal when the input signal is white noise is the 2-norm of the transfer function. In Figure 15 the RMS of the output signal f_1 is plotted against the RMS value of the control output v_1. The two inputs w_d and w_m are zero-mean white noise processes with variances of 1 and 100. For different values of ρ we calculated the RMS values of the output signals. Increasing ρ forces less control action and thus a lower RMS value. There is a clear trade-off between the two terms. If more control action is allowed, less disturbance comes through the system. Less control energy also implicates more deviations on the air flow rate.

The design corresponding to $\rho = 1$, is obviously one of the best designs, since RMS(f) and RMS(u) are both low. Changing ρ yields a drastic change in RMS(f) or the need for much more energy. A good design has to be situated in the left-hand corner of the curve.

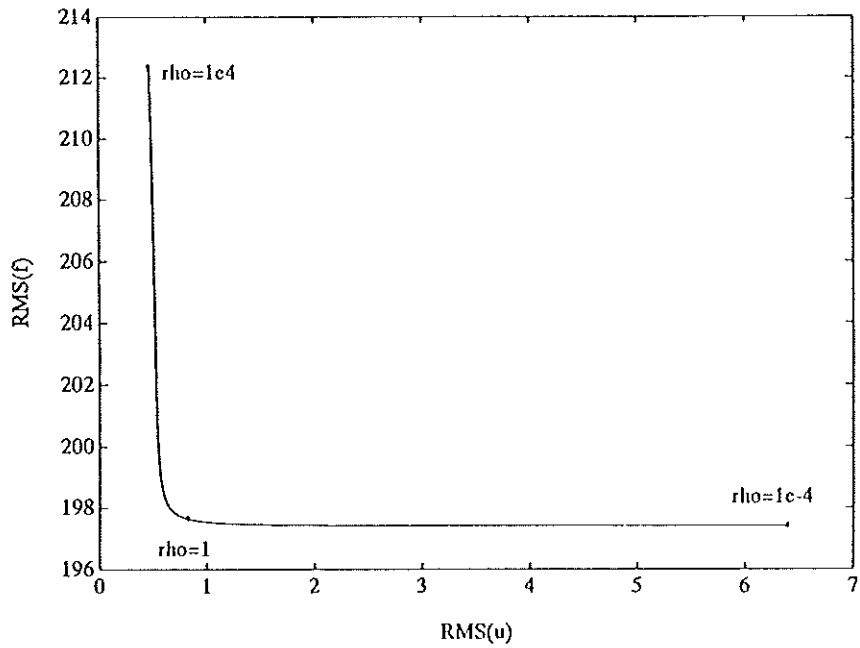


Figure 15. Trade-off between the RMS values of the control signal and the output

5.4. Robustness versus the control energy

Here is another trade-off: robustness against the control energy. The more robust the design has to be, the less control energy is allowed. In Figure 16 the D-circle and M-circle are plotted against RMS(u) for the H_2 controller.

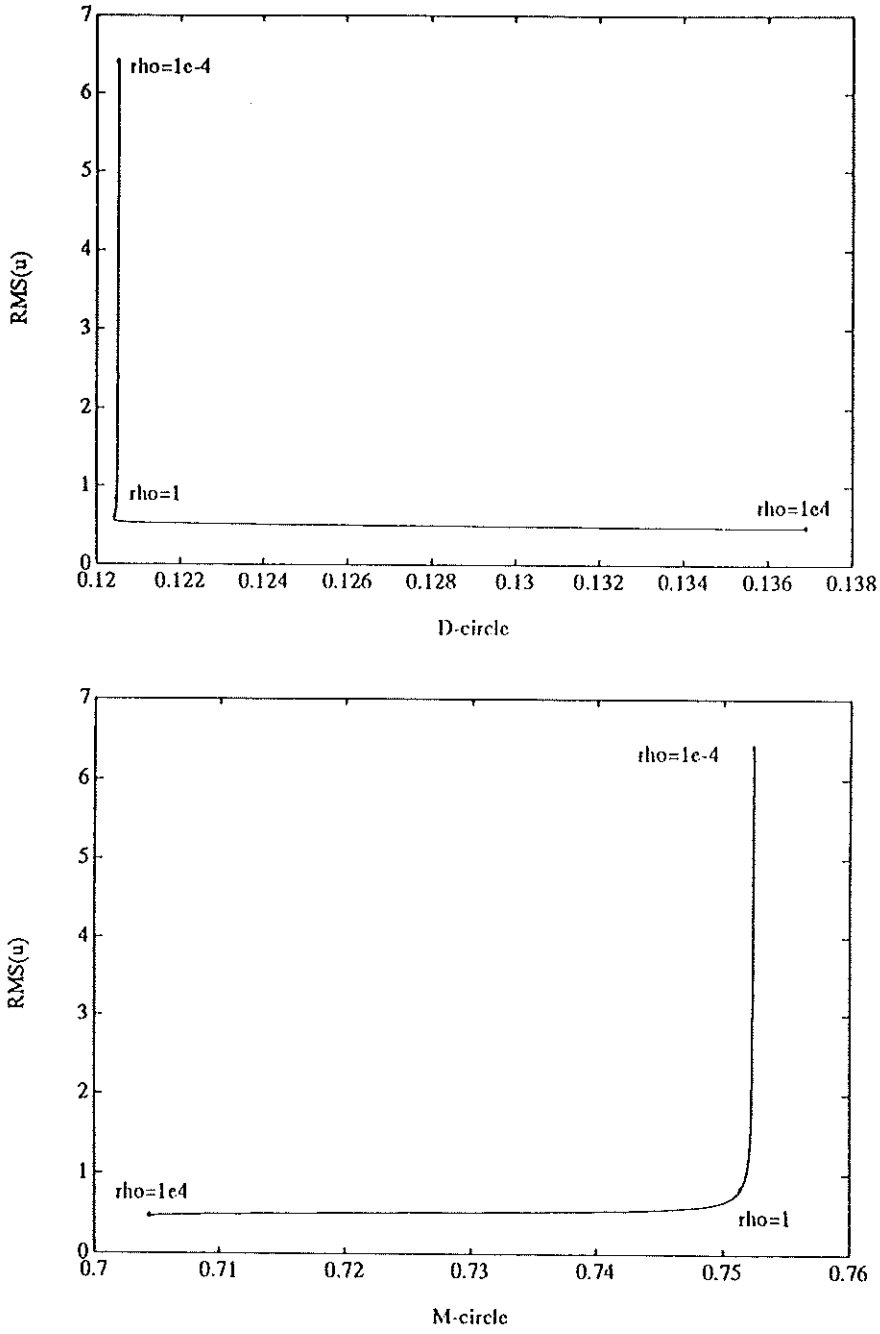


Figure 16. The D-circle versus RMS(u) and the M-circle versus RMS(u) for H_2 controller designs for different values of ρ ($10^{-4} \leqslant \rho \leqslant 10^{4}$). RMS($u$) should be as low as possible and the D-circle as low as possible. These conditions are co-operating and do not form a trade-off. However, the M-circle should be as large as possible while RMS(u) should be minimized. This a trade-off

RMS(u) and the M-circle form a trade-off. The M-circle should be as large as possible. However, from a certain moment on RMS(u) increases dramatically, whereas for a good design a small RMS(u) is desired. RMS(u) and the D-circle, however, do not form a trade-off: the larger the D-circle, the smaller the RMS(u) is. This indicates that when the M-circle forms a trade-off with the D-circle and RMS(u), the last two will change together.

5.5. Motivation for installing better measurement equipment

By computer simulation we can also motivate the need for better measurement equipment. The flow measurer used had a noise input and the variance was taken to be 100. Better measurement equipment will make the variance σ_m^2 of the measurement noise smaller. By computer simulation it is easy to see what will happen when σ_m changes. This is shown in Figure 17 for the ∞-norm. Decreasing σ_m also leads to lower norms on the overall transfer function both for the H_∞ and H_2 controller.

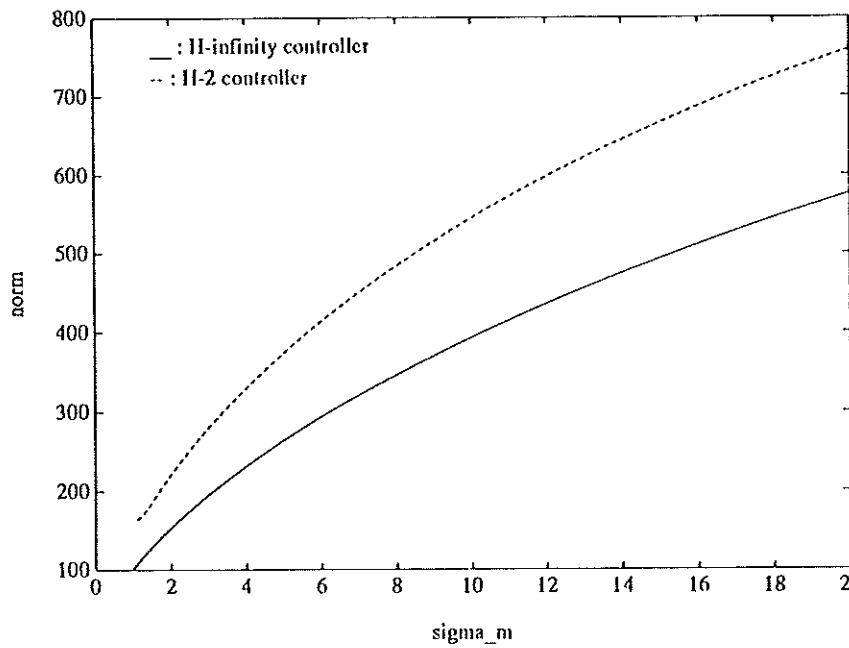


Figure 17. The ∞-norm of H_{fw} as a function of σ_m ($w = [p_1\ w_m]^T$). Obviously, installing better measurement equipment, thus giving a lower σ_m, improves the ∞-norm of both the H_∞ and H_2 designs

6. CONCLUSIONS

In this paper we have shown how to obtain a general performance analysis of a simple realistic control problem. Most modern control techniques are model-based. If possible, not only the system should be modelled but also the disturbances and sensors. All these models can be combined in one generalized plant which is used for the controller calculation. Modern control design techniques thus have the possibility of taking into account all available information about the controlled process.

Since we are dealing with linear time-invariant systems, some fundamental constraints are present, e.g. Bode's integral. This implies that we cannot have disturbance rejection over the full $j\omega$-axis. Increasing the disturbance rejection in one frequency interval will make it worse in another.

The design of linear controllers is also subject to a lot of trade-offs. Improving certain criteria will make others worse. In the paper we showed e.g. the trade-off between the M-circle and D-circle and between the M-circle and the RMS of the actuator signal.

The whole analysis shows that CACSD is a very useful tool in the design of linear controllers. Several controllers can be calculated quickly and their performances compared. The designer can also get some idea about the limitations on his design. However, despite all mathematical machinery, the control engineer still needs to rely on his common sense to obtain a good design.

ACKNOWLEDGEMENTS

Some of the results presented in this paper have been obtained within the framework of the Belgian Program on Concerted Research Actions and on Interuniversity Attraction Poles initiated by the Belgian State, Prime Minister's Office, Science Policy Programming. The scientific responsibility rests with its authors. Partial funding was also provided by the Research Council of the Katholieke Universiteit Leuven. Dr De Moor and Dr Berckmans are research associates of the Belgian National Fund for Scientific Research (NFWO). Johan David is a research assistant with the NFWO.

REFERENCES

1. Barratt, C. and S. Boyd, 'Example of trade-offs in linear controller design', *Control Syst. Mag.*, 9, 46–52 (1989).
2. Boyd, S. and C. Barratt, *Linear Controller Design: Limits of Performance*, Prentice-Hall, Englewood Cliffs, NJ, 1990.
3. Boyd, S., V. Balakrishnan, C. Barratt, N. Khraishi, X. Li, D. Meger and S. Norman, 'A new CAD method and associated architectures for linear controllers', *IEEE Trans. Automatic Control*, 33, 268–283 (1988).
4. *MATLAB, User's Guide*, The MathWorks, South Natick, MA, 1990.
5. *MATRIX$_X$, Device Specific Information*, Integrated Systems, 1989.
6. De Moor, B., J. David, J. Vandewalle, M. De Moor and D. Berckmans, 'Trade-offs in linear control system design: a practical example', *ESAT-SISTA Report 1991-04*, Department of Electrical Engineering, Katholieke Universiteit Leuven, Leuven, 1991.
7. De Moor, B., J. Swevers and H. Van Brussel, 'Stepped sine system identification, errors-in-variables and the quotient singular value decomposition', *Mechanical Systems and Signal Processing 6*, November, pp. 121–134 1992.
8. Kuo, B. C., *Automatic Control Systems*, 5th edn, Prentice-Hall International, Englewood Cliffs, NJ, 1987.
9. Ziegler, J. G. and N. B. Nichols, 'Optimum settings for automatic controllers', *Trans. ASME*, 64, 759–768 (1942).
10. Anderson, B. D. O. and J. B. Moore, *Optimal Control—Linear Quadratic Methods*, Prentice-Hall, Englewood Cliffs, NJ, 1989.
11. Doyle, J., 'Advances in multivariable control', *Lecture Notes at ONR/Honeywell Workshop*, Minneapolis, MN, October 1984.
12. Kwakernaak, H. and R. Sivan, *Linear Optimal Control Systems*, Wiley, 1972.
13. Francis, B. A., *A Course in H_∞ Control Theory, Lecture Notes in Control and Information Sciences*, 88, Springer, Heidelberg, 1987.
14. Glover, K. and J. Doyle, 'State-space formulae for all stabilizing controllers that satisfy an H_∞-norm bound and relations to risk sensitivity', *Syst. Control Lett.*, 11, 167–172 (1988).
15. Doyle, J., K. glover, P. P. Khargonekar and B. A. Francis, 'State-space solutions to standard H_2 and H_∞ control problems', *IEEE Trans. Automatic Control*, AC-34, 831–847 (1989).
16. Glover, K., D. J. N. Limebeer, J. C. Doyle, E. M. Kasenally and M. G. Safanov, 'A characterisation of all solutions to the four block general distance problem', *SIAM J. Control Optim.*, 29, 283–324 (1991).

17. Moore, B. C., 'Principal component analysis in linear systems: controllability, observability, and model reduction', *IEEE Trans. Automatic Control*, **26**, 17–31 (1981).
18. Glover, K., 'All optimal Hankel-norm approximations of linear multivariable systems and their L_∞-error bounds', *Int. J. Control*, **39**, 1115–1193 (1984).
19. Jonckheere, E. A. and L. M. Silverman, 'A new set of invariants for linear systems—application to reduced order compensator design', *IEEE Trans. Automatic Control*, **28**, 853–964 (1983).
20. Boyd, S. and C. A. Desoer, 'Subharmonic functions and performance bounds on linear time-invariant feedback systems', *IMA J. Math. Control Info.*, 153–170 (1985).
21. Zames, G., 'Feedback and optimal sensitivity: model reference transformations, multiplicative seminorms, and approximate inverses', *IEEE Trans. Automatic Control*, **AC-26**, 301–320 (1981).
22. Doyle, J. 'Analysis of feedback systems with structured uncertainties', *Proc. IEE*, **129**, pt. D, 242–250 (1982).